- Technical Paper -

FRACTURE MECHANISMS IN SPLIT-TENSILE TEST OF FRC BY AE-SiGMA ANALYSIS

M. R. I. A. J. MONDORINGIN[*1] and Masayasu OHTSU[*2]

ABSTRACT

Fracture mechanisms of fiber reinforced concrete in the split-tensile tests are studied. In comparison with control specimens of normal concrete, reinforced concrete samples by steel-fiber are tested. Mechanisms of tensile fracture at the meso-scale is identified by applying the SiGMA (Simplified Green's functions for Moment tensor Analysis) analysis to the split-tensile tests. In the Stage 1 of macro-scale fracture, a few AE events are observed and tensile cracks are less dominant than those of normal concrete due to the reinforcing effect of fiber. In the Stage 2, shear cracks and other than tensile cracks are more actively observed than those of normal concrete. This demonstrates that pulling-out of fibers and fretting of cracked surfaces result in AE activity in SFRC.
Keywords: split-tensile test, steel fiber, tensile strength, crack kinematics

1. INTRODUCTION

The moment tensor analysis of AE waveforms has been developed and is now available for identifying crack kinematics of a location, a crack-type and a crack orientation in cioncrete. The procedure has been implemented as the SiGMA (**Si**mplified **G**reen's functions for **M**oment tensor **A**nalysis) analysis [1]. It is demonstrated that mechanisms of cracking can be visually and quantitatively studied at the meso-scale in concrete.

Since the tensile strength of concrete is normally evaluated by the split-tensile (Brazilian) test, mechanisms of macro-scale tensile failure in concrete have been studied as the cracking process at the meso-scale as determined by the SiGMA analysis [2]. Evolution of the fracture process zone under the combination of tensile and compressive stresses is discussed.

Further we have clarified a theoretical basis on the agreement of the tensile strengths of normal concrete in the split-tensile test and the direct tensile test, by applying the SiGMA analysis [3]. The facture process zone is created in a cross-section under constant tensile stress in the both tests. Thus, it is clarified that similar nucleation processes of the facture process zone could reasonably lead to comparable tensile strengths in the split-tensile test and the direct tensile.

Recently, it is reported that the tensile strength of fiber-reinforced concrete is not straightforward to be estimated in the split-tensile test [4]. In this respect, fracture mechanisms of fiber-reinforced concrete in the split-tensile test are to be clarified at the meso-scale. In the present paper, the SiGMA analysis is applied to the split - tensile tests of steel - fiber reinforced concrete (SFRC), and results are compared with those of normal concrete

2. TEST PROGRAMS

2.1 Materials

Mixture proportions of concrete tested are given in Table 1, where mixture proportion of SFRC is based on the normal concrete. The maximum gravel size is 20 mm. By employing the ordinary Portland cement, straight -steel fiber of 30 mm length was added by 0. 1 % of concrete volume for SFRC. According to the target design, slump and air content was controlled as 8 cm and 6 %, respectively, by using air - entrained admixture. For each mixture, 3 cylindrical specimens of 100 mm diameter and 200 mm length were made for the compression test. For the split-tensile test, one specimen of 150 mm diameter and 300 mm length were made. They were demoulded after 24 hours and moisture-cured in the standard room at 20^{o} Celsius. After 28-day moisture-curing, the compression tests were conducted. The specimen for the split-tensile test was cut into 2 specimens of 100 mm length and the tests were conducted for 4 specimens. Compressive and tensile strengths averaged of all specimens are summarized in Table 2.

2.2 Test Procedure

AE signals were detected by employing AE Win SAMOS (PAC). Eight AE sensors of 150 kHz resonance (R151-AST) were attached to the specimen.

Table 1 Mixture proportions of concrete

Concrete	W/C	Slump (cm)	s/a (%)	Weight per unit volume (kg/m3)				
				W	C	S	G	Fiber
Normal	0.55	7.7	44	173	314	757	1144	-
SFRC	0.55	7.0	44	173	314	757	1135	23.4

*1 Graduate School of Science and Technology, Kumamoto University, JCI Student Member
*2 Prof., Graduate School of Science and Technology, Kumamoto University, JCI Member

Table 2 Strengths of concrete

Concrete	Compressive strength (MPa)	Tensile strength (MPa)
Normal	23.9	2.30
SFRC	25.2	2.49

The frequency range was from 10 kHz to 2 MHz and total amplification was 60 dB gain (40 dB gain in a pre-amplifier and 20 dB in a main amplifier). Prior to the test, the sensor array was determined by a simulation analysis [3]. Eight sensors were arranged on the surface of the specimen as shown in Fig. 1 and their coordinates with respect to the coordinate system in Fig. 1 are given in Table 3.

2.3 AE-SiGMA Analysis

A simplified procedure to determine the moment tensor components from AE waveforms in a multi-channel AE system is developed and the eigen-value analysis of the moment tensor is applicable to determine crack type and orientation [1]. The eigen-values of the moment tensor are to be composed of the combination of the shear crack and the tensile crack.

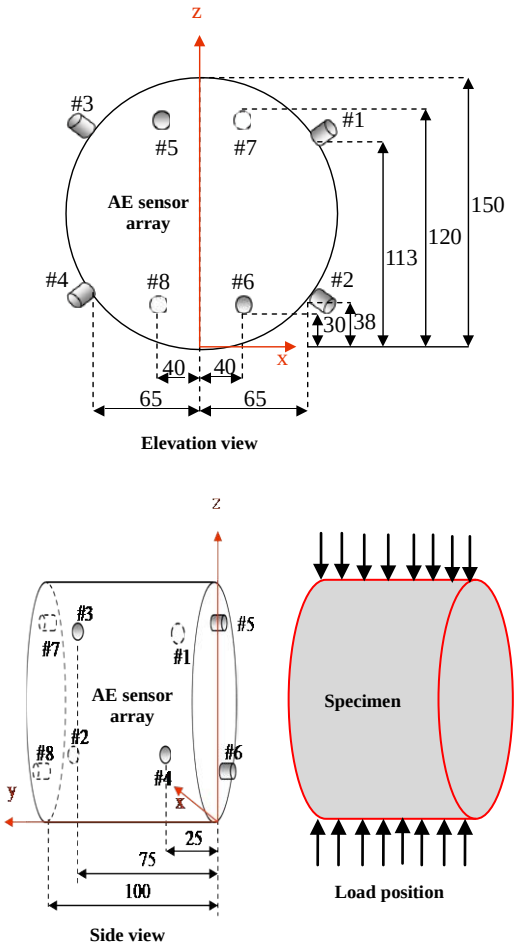

Fig. 1 Specimen, AE sensor array and load position

Table 3 Coordinates of AE sensors

Sensor coordinates	x (m)	y (m)	z (m)
Channel 1	0.065	0.025	0.113
Channel 2	0.065	0.075	0.038
Channel 3	-0.065	0.075	0.113
Channel 4	-0.065	0.025	0.038
Channel 5	-0.040	0.000	0.120
Channel 6	0.040	0.000	0.030
Channel 7	0.040	0.100	0.120
Channel 8	-0.040	0.100	0.030

Thus, decomposition of the eigen-values leads to the shear component (X), the deviatoric tensile component (Y), and the hydrostatic component (Z) of the tensile crack. components correspond to CLVD and the equivalent stresses to the crack volume. In the present SiGMA code, AE source with the shear ratio X > 60 % is classified as the shear crack, one with X < 40 % as a tensile crack and one with 40 % < X < 60 % as a mixed-mode crack. The crack-motion vector and the normal vector are determined from three eigenvectors. Results are visually displayed, by using a graphic software (Light Wave 3D, New Tek). Three models of these cracks are illustrated in Fig. 2. Cracks are classified into three types of shear, mixed-mode and tensile, and their crack planes normal to vectors are illustrated by circles and directions of crack motions are shown by arrows.

It is worth to note a relationship with the modes in linear fracture mechanics. Although the crack classification of the tensile crack and the shear crack in the SiGMA analysis was referred to as identical to mode I and mode II in fiber-reinforced concrete [5], the treatment is not rational. Rigorously speaking, the crack classification by the moment tensor is based on crack displacements (motions) on the crack surface at the meso-scale. In contrast, the modes in fracture mechanics represent crack propagation from the crack-tip at the macro-scale in composite materials. In the case that crack orientation θ is taken into account for crack propagation, the modes can be calculated from the criterion on the crack extension [6],

$$K_I \sin\theta + K_{II}(3\cos\theta - 1) = 0, \qquad (1)$$

$$\cos\frac{\theta}{2}\left(K_I \cos^2\frac{\theta}{2} - \frac{3}{2}K_{II}\sin\theta\right) = K_{IC}. \qquad (2)$$

Here K_I and K_{II} are the stress intensity factors of mode I and mode II, respectively. K_{IC} is the critical stress Intensity factors of mode I

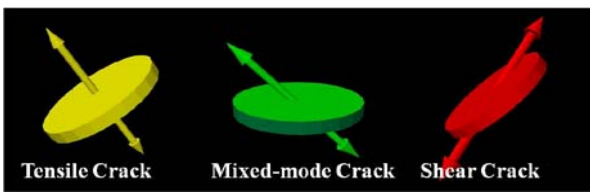

Crack models

Referring to the propagation angle θ as the angle between consecutive AE sources determined from normal vectors, the extension of tensile cracks due to volumetric expansion in concrete was studied, applying Eqs. 1 and 2. It was found that the extension of the tensile cracks at the macro-scale is dominantly governed by mode I failure, even though all the types of tensile, mixed-mode and shear cracks were observed at the meso-scale in the SiGMA analysis [7].

In the SiGMA analysis, the determination of the two parameters of the arrival time and the amplitude of the first motion is essential and previously carried out by visual and hand-picking. To improve these enormous efforts for the analysis, we have currently developed an automated detection method based on AIC (Akaike Information Criteria) [8].

2.4 Theory of Split-Tensile Test

Theoretical basis for stress distribution in the split-tensile test is well developed [5] as a stress analysis of a disc subjected to two concentrated diametrical forces assuming the plane stress. At the center of the disc, the following equations on the horizontal stress σ_{xx}, the vertical stress σ_{yy} and the shear stress τ_{xy} are obtained;

$$\sigma_{xx} = \frac{2P}{\pi DL} \quad (3)$$

$$\sigma_{yy} = -\frac{6P}{\pi DL} \quad (4)$$

$$\tau_{xy} = 0 . \quad (5)$$

Here P is the applied load, L is the thickness of the disc, and D is the diameter of the disc. The tensile strengths in Table 2 are obtained from Eq. 3.

3. RESULTS AND DISCUSSION

After the split-tensile tests, it is found that AE results of the two specimens are similar. Therefore, results of the one specimen, in which we observed more AE hits and events, are discussed here-in-after.

3.1 Normal Concrete

A relation between load and AE activity is shown in Fig. 3. As found in the previous research [2], AE hits, which imply the number of AE waves counted by all AE sensors, are actively observed at only the final stage. The stage corresponds to nucleation of the fracture process zone and crack extension from the through-diameter crack at the macro-scale on one end to the whole cross-section. As observed in Fig. 3, a few AE hits are observed until 25 kN applied load. Then, in between 25 kN to 50 kN of applied load, AE hits increase gradually. Eventually, they reach their peak at 52 kN. Consequently, the fracture process is classified into three stages as illustrated as Stage 1, Stage 2, and Stage 3. AE waves of which the first motions were successfully detected at all 8 channels were analyzed to locate AE sources and then the SiGMA analysis was performed. These are named as

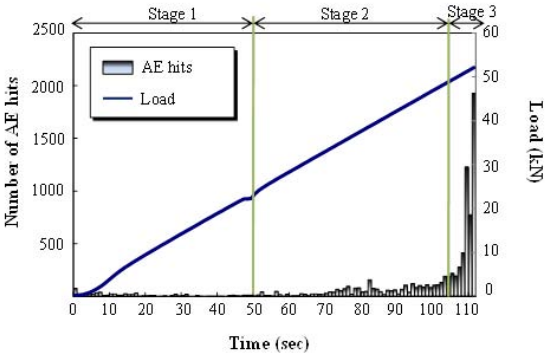

Fig. 3 Load-AE hits relation (normal concrete).

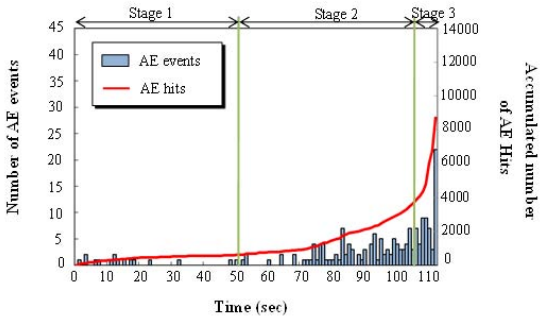

Fig. 4 AE activity and three stages (normal concrete).

AE events. In Fig. 4, AE events analyzed are plotted along with the curve of accumulated AE hits. As classified to 3 stages, a few AE events are analyzed in Stage 1, where micro-cracking occurs. The number of AE events increases towards Stage 2 and Stage 3, where AE activity are high and matrix macro cracking occurs. At each stage, results of SiGMA analysis are illustrated in Fig. 5. At Stage 1, only 6 events are plotted. They are located around the top and the bottom zones of the specimen, suggesting crack nucleation at the meso-scale near the loading plates. AE activity near the loading plates are further accelerated at Stage 2. All the types of cracks at the meso-scale are mixed up.

Toward the final at Stage 3, cracks are coalesced and propagate onto the whole cross-section. Here, AE events in total are shown. As shown in Fig. 5 (c), AE cluster at the elevation view is in remarkable agreement with the final tensile crack at the macro-scale, which is marked by the white line. The fact actually suggests that the fracture process zone is created around the final crack surface.

In order to investigate the fracture process of normal concrete in the split-tensile test, ratios of the tensile, mixed-mode and shear cracks are compared in Fig. 6. It is found that the number of analyzed events gradually increases from Stage 1 to Stage 3. Concerning the ratios, the number of tensile cracks is compatible to that of mixed-mode plus shear cracks. Referring to the mixed-mode cracks as other than tensile cracks, it is realized that a half of cracks nucleated are tensile cracks at the meso-scale in the split-tensile test of normal concrete.

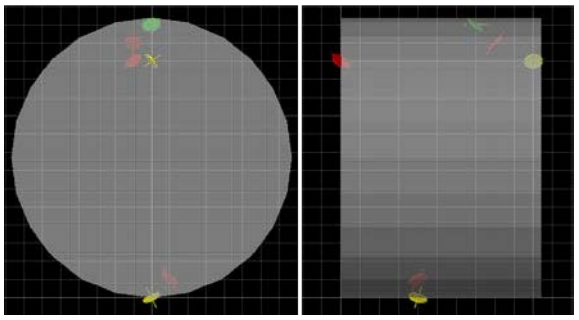

(elevation view) (side view)

(a) Stage 1

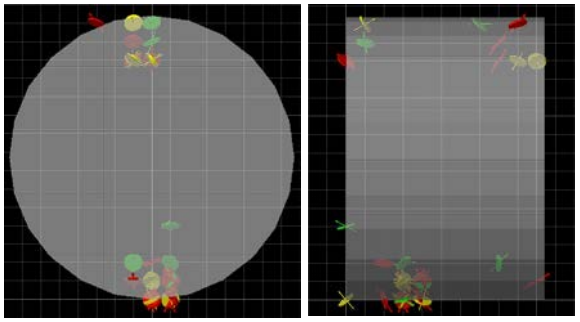

(elevation view) (side view)

(b) Stage 2

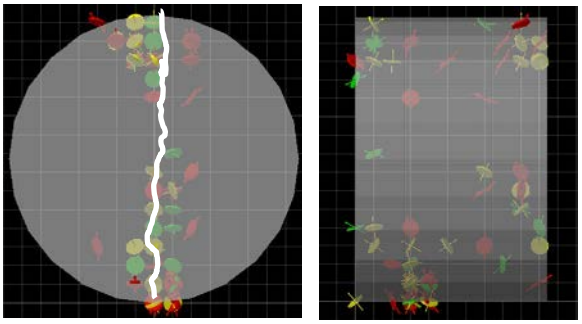

(elevation view) (side view)

(c) Stage 3 (in total)

Fig. 5 Results of SiGMA analysis (normal concrete).

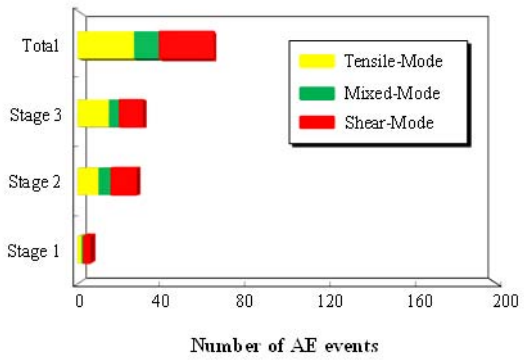

Fig. 6 Crack modes analyzed by SiGMA in normal concrete.

3.2 Steel-Fiber reinforced Concrete

The relation between load and AE hits is illustrated in Fig. 7. AE activity under loading is quite similar to Fig. 3, and again is classified into three stages. It is clearly observed that AE activity at Stage 3 is even higher than that of normal concrete. This suggests that more cracks are generated at the final stage. Before reaching around 42 kN of applied load at Stage 1, few AE hits are observed and thus cracks at the meso-scale are prevented by the reinforcing effect of fibers. In between 42 kN to 56 kN of applied load at Stage 2, AE hits are steadily observed. The fact might be associated with crack growth, which is somehow restricted by fibers. At Stage 3, AE hits are acceleratedly generated.

The relation between accumulated number of AE hits and AE events is shown in Fig. 8. Generating trend of AE events is similar to that of AE hits. So, it is understood that quite actively AE sources are observed at only Stage 3. These AE sources possibly result from pulling-out of fibers, extension of tensile cracks and fretting of cracked surfaces.

Results of the SiGMA analysis are illustrated in Fig. 9. In total, 160 AE events are detected and analyzed. At Stage 1, tensile-mode and mixed-mode cracks are dominant with 19 AE events in total, while only 5 AE events of shear cracks are detected. At Stage 2, the number of shear cracks increase gradually.

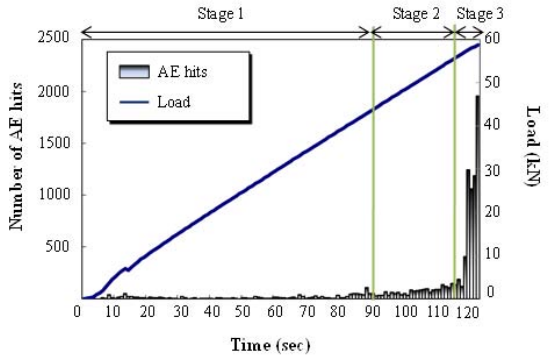

Fig. 7 Load-AE hits relation (SF concrete).

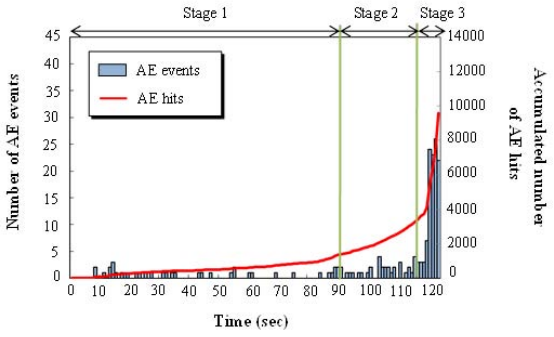

Fig. 8 AE activity and three stages (SF concrete)

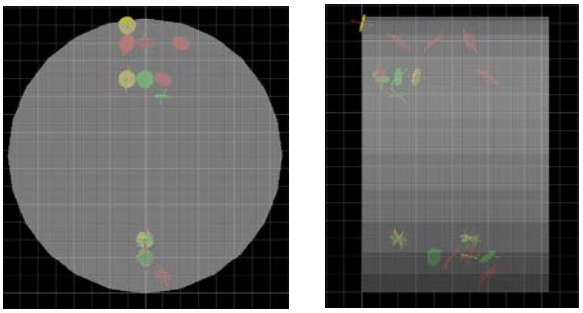

(elevation view) (side view)

(a) Stage 1

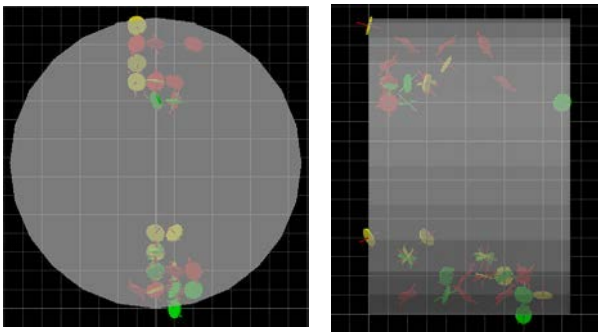

(elevation view) (side view)

(b) Stage 2

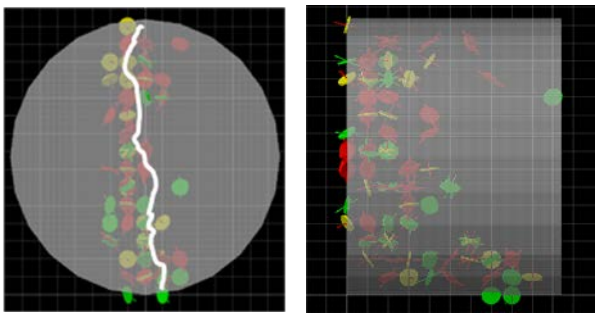

(elevation view) (side view)

(c) Stage 3 (in total)

Fig. 9 Results of SiGMA analysis (SF concrete)

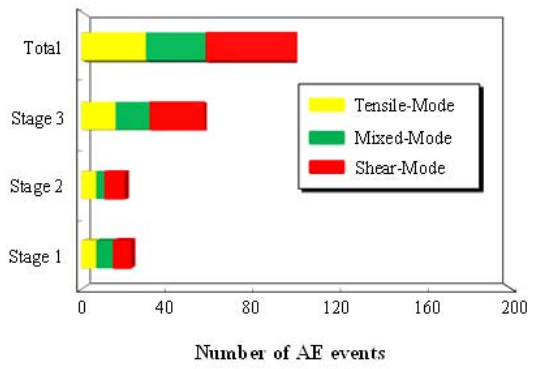

Fig. 10 Crack modes analyzed by SiGMA in SF concrete.

At both Stage 1 and Stage 2, AE sources are only observed around the loading plates at the top and the bottom of the specimen. This implies that the fracture process zone is not completely created. Cracks at the macro-scale are still under extension toward the central zone of the specimen. At Stage 3, AE sources are intensely observed at the left side of the specimen in Fig. 9 (c). Since the load was quickly released after the main crack at the left-side circular surface was observed. Crack distribution in the figure is biased at the left side in the side view. So, this might correspond to the stage under development of the fracture process zone. As a matter of course, the location of the main crack is in remarkable agreement with AE cluster.

The ratios of the tensile, mixed-mode and shear cracks are compared in Fig. 10. It is found that the number of analyzed events at Stage 1 is similar to that of Stage 2, where the number of tensile cracks and mixed-mode is comparable to that of shear cracks. In comparison with Fig. 6, the dominant increase of AE events is emphasized. Based on discussion before-mentioned, the number of the mixed-mode cracks is taken into account as other than tensile cracks. It is realized that the number of AE sources other than tensile cracks including shear cracks is definitely dominant at Stage 3, suggesting nucleation of pulling-out fibers and fretting crack-surfaces created. Thus, under development of the fracture process zone in fiber-reinforced concrete, meso-scale cracks other than tensile cracks are actively generated in the spli-tensile test. According to the study by Denneman et al. [4], two peaks of the loading curve are discussed, and they conclude that the first peak load should be applied to Eq. 3 to estimate the tensile strength of fiber-reinforced concrete. Because the first peak might be observed following Stage 2, this strength could correspond to the strength of concrete constrained by fibers.

4. CONCLUSIONS

The following conclusions can be drawn from this study.

(1) Mechanisms of macro-scale tensile failure process in concrete are clarified as the crack accumulation process at meso-scale determined by the SiGMA analysis.
(2) There exist three stages on nucleation of AE sources at the meso-scale in the split-tensile test for the tensile strength of concrete.
(3) In comparison with the fracture process in normal concrete, the bridging mechanisms of fibers are suggested, as fibers can restrain the crack propagation in concrete.
(4) The mechanism above is demonstrated as the dominant generation of the meso-scale cracks aother than tensile cracks at Stage 3.
(5) According to the previous study, out of two peaks of the loading curve, the first peak load is recommended to estimate the tensile strength of fiber-reinforced concrete.

Because the first peak might be observed following Stage 2, this strength could correspond to the strength of concrete constrained by fibers.

ACKNOWLEDGEMENT

The research conducted is supported by Kumamoto University Global COE (Center of Excellence) Program: Global Initiative Center for Pulsed Power Engineering. To perform experiments and analyses, the assistances of technical associate, Dr. Yuichi Tomoda and Graduate student, Mr. Yuma Kawasaki are highly valuable. The authors wish to deeply thank the program and their support.

REFERENCES

[1] Ohtsu M, Okamoto T, and Yuyama S. (1998),"Moment Tensor Analysis of AE for Cracking Mechanisms in Concrete," ACI Structural Journal, 1998, 95(2), pp. 87-95.

[2] Mondoringin, M, Nozaki, S. and Ohtsu, M.,"AE-SiGMA Analysis in Brazilian Test of Concrete ", Concrete Research Letters, 2 (3), 2011, pp. 267-270.

[3] Ohtsu, M., Nozaki, S. and Kawasaki, Y.,"AE-SiGMA Analysis in Split-Tensile Test of Concrete," Concrete Research and Technology, JCI, 22(3), 2011, pp. 27-34.

[4] Denneman, E., Kearsley, E. and Visser, A.,"Splitting Tensile Test for Fiber Reinforced Concrete," Materials and Structures, 44(8), 2011, pp. 1441-1449.

[5] Carpinteri, A., Lacidogna, G. and Manuello, A.,"An Experimental Study on Retrofitted Fiber-Reinforced Concrete Beams using AE, Fracture Mechanics of Concrete and Concrete Structures, Taylor & Francis, London, Vol. 2, 2007, pp. 1061-1068.

[6] Erdogan, F. and Sih, G. C.,"On the Crack Extension in Plates under Plane Loading and Transverse Shear," J. Basic Eng., 12, 1963, 519-527.

[7] Ohtsu, M. and Uddin, F. A. K. M.,"Mechanisms of Corrosion-Induced Cracks in Concrete at Meso- and Macro-Scales," Jourbnal of ACT, **6**(3), 2008, pp. 419-429.

[8] Ohno, K. and Ohtsu, M.,"Crcak Classification in Concrete based on AE," Construction and Building Materials, **24**(12), 2010, pp. 2339-2346.